Temperatures above thermal optimum reduce cell growth and silica production while increasing cell volume and protein content in the diatom *Thalassiosira pseudonana*

Cristin E. Sheehan[1], Kirralee G. Baker[2], Daniel A. Nielsen[1], Katherina Petrou[1]

[1]School of Life Sciences, University of Technology Sydney, Sydney, NSW, Australia.

[2]School of Life Sciences, University of Essex, Wivenhoe Park, United Kingdom.

*Author for correspondence: Katherina Petrou

Phone: +61 2 95144159

Email: Katherina.Petrou@uts.edu.au

Abstract

Temperature plays a fundamental role in determining phytoplankton community structure, distribution, and abundance. With climate models predicting increases in ocean surface temperatures of up to 3.2°C by 2100, there is a genuine need to acquire data on the phenotypic plasticity, and thus performance, of phytoplankton in relation to temperature. We investigated the effects of temperature (14 - 28 °C) on the growth, morphology, productivity, silicification and macromolecular composition of the marine diatom *Thalassiosira pseudonana*. Optimum growth rate and maximum P:R ratio were obtained around 21 °C. Cell volume and chlorophyll *a* increased with temperature, as did lipids and proteins. One of the strongest temperature-induced shifts was the higher silicification rates at low temperature. Our results reveal temperature-driven responses in physiological, morphological and biochemical traits in *T. pseudonana*; whereby at supra-optimal temperatures cells grew slower, were larger, had higher chlorophyll and protein content but reduced silicification, while those exposed to sub-optimal temperatures were smaller, heavily silicified with lower lipid and chlorophyll content. If conserved across species, our findings indicate that as oceans warm, we may see shifts in diatom phenotypes and community structure, with potential biogeochemical consequences of higher remineralisation and declines in carbon and silicon export to the ocean interior.

Keywords: phenotypic traits; thermal performance curves; climate change; diatoms; silicification; macromolecules

Introduction

Temperature defines the biogeographical boundaries and distribution of major groups of phytoplankton (Longhurst 2010), but with ocean temperatures predicted to warm between 1.2-3.2 °C by 2100 (Gattuso et al. 2015; Meehl et al. 2007), changes to phytoplankton biogeography are expected. As temperature zones shift due to climate change, we are seeing the displacement of local or regional species by species that are better suited to the new environmental conditions (Barton et al. 2016; Burrows et al. 2014). While spatial changes in ocean temperature could lead to altered species distributions, temporal changes could affect the timing of spring blooms (Edwards and Richardson 2004; Gao et al. 2012). To gain insight into how species distribution and productivity might shift, and whether or not these shifts will alter the functionality of phytoplankton, either through changes in nutritional value, grazing or sinking rates, it is useful to explore phenotypic responses of model organisms to environmental gradients such as temperature.

Diatoms make excellent model organisms for assessing phytoplankton trends. Globally distributed and responsible for more than 40% of all ocean carbon fixation, diatoms are major contributors to global primary production and play a significant role in the ocean's biological pump, removing CO_2 from near surface waters to ocean depths (Tréguer et al. 2018; Tréguer and De La Rocha 2013). As major primary producers, they also influence biogeochemical cycling of elements, accumulating macronutrients and trace metals such as N, P, Si and Fe, which either sink to depth, are remineralised in surface waters or are consumed by higher trophic levels (Falkowski et al. 1998; Twining et al. 2008). Diatoms are distinguished from other phytoplankton groups by their frustules, a distinctive two-part cell wall made of hydrated silicon dioxide (Martin-Jezequel et al. 2000). Producing an estimated 6 Tmol Si $year^{-1}$, diatoms are the primary manufacturers of biogenic silica and an essential component of the marine silicon cycle (Treguer et al. 1995; Tréguer and De La Rocha 2013).

Phytoplankton growth rate in response to temperature is often described by a bell-shaped curve, however due to evolved gene expression, phenotypic acclimation to temperature changes vary between species and strains (Boyd et al. 2013; Huertas et al. 2011; Liang et al. 2019; Suzuki and Takahashi 1995). The bell shape emerges as organisms exposed to sub-optimal temperatures are warmed towards their optima. This increase in growth temperature results in a positive effect on photosynthesis and cell division, which can be explained by the enhancement of enzymatic activities, particularly those associated with the Calvin cycle. As temperatures exceed the thermal optimum however, growth rate sharply decreases. This is often attributed to heat stress and the detrimental effect it can have on enzyme function and proteins involved in photosynthesis (Mathur et al. 2014; Salvucci and Crafts-Brandner 2004), thereby inhibiting growth.

The nutritional value of phytoplankton and how efficiently biomass can be transferred between trophic levels is reliant on phenotypic characteristics including morphology, biochemical composition, and digestibility (Brown 2002; Thompson et al. 1992; Van Donk et al. 2011). Studies on the biochemical composition of phytoplankton have shown temperature can affect lipid, protein and carbohydrate content of cells. When grown above or below their optimum temperature microalgae experience a decrease in total lipid content (Converti et al. 2009), and at lower temperatures cell membrane can become more rigid causing an increase in the production of unsaturated fatty acids to increase membrane fluidity (Juneja et al. 2013; Renaud et al. 2002). Temperature has also been shown to affect protein content in microalgae, however the direction of change is variable and it has been suggested to be dependent on the evolutionarily defined thermal history of the strain being tested (Liang et al. 2019). Growth morphology and cell size also influence trophic energy transfer efficiency and both attributes

have been linked to carbon export from surface waters, whereby larger, chain forming or aggregating cells, are associated with greater sinking rates, and thus greater carbon export (Finkel et al. 2009). With diatoms, silica content is an important consideration, whereby larger cells generally have more silica, and therefore sink more readily, as silica has a higher density than seawater (Smetacek 2000). However, studies on diatom clones grown at a range of temperatures, have shown decreased silicification rates at warmer temperatures (Baker et al. 2016), indicating thinner frustules, which would reduce sinking rates by decreased density and increased grazing potential (Raven and Waite 2004).

In light of the complexity surrounding temperature-driven phenotypic responses in phytoplankton, there is a need to better understand how temperature influences growth, macromolecular composition and silica accumulation in concert, as even small changes to any or all of these traits has the potential to alter trophic dynamics, as well as carbon and silica fluxes throughout the global ocean. In this study, we investigate phenotypic traits, including growth, cell size, chlorophyll content and productivity in the model diatom species *T. pseudonana* acclimated to eight temperatures (14 - 28°C). We then combine those traits with measured changes in silica deposition rates and macromolecular composition to better understand the potential influence of ocean warming on diatom fitness, trophic energy transfer and the biological pump.

Methods

Culturing and experimental protocol

The marine centric diatom *Thalassiosira pseudonana* (Hustedt) Hasle et Heimdal used in this study was originally isolated from the Swan River Estuary in Western Australia and was obtained from the Australian National Algae Culture Collection (CSIRO – strain CS-20).

126 Cultures were grown in sterilised glass Erlenmeyer flasks containing 0.22 µm filter sterilised
127 natural seawater enriched with F/2 medium (Guillard and Ryther 1962) and maintained in a
128 temperature controlled incubator at 20 °C under a 12:12 hour light:dark cycle with light
129 provided at 100 µmol photons m^{-2} s^{-1}. For the present experiment, aliquots of *T. pseudonana*
130 were transferred into 75 cm^2 sterile tissue culture bottles (n = 4)and incubated in aquaria under
131 controlled temperature conditions. Tanks were kept at constant temperatures (14, 16, 18, 20,
132 22, 24, 26 and 28°C) using heater/chillers (Julabo, Germany) and monitored for the entire
133 experimental period using submersible temperature sensors (Thermochron iButton, United
134 States), logging temperature every 5 min (Table 1). Programmable 150W LED aquarium lights
135 (with a 1:1 mix of blue (470 nm) and white (8000K) LEDs; Phantom CIDLY, China) were
136 positioned at a set distance along the front side of the tanks. The lights were programmed using
137 a 16-step light curve to simulate a natural diel cycle (12:12, L:D) with a daily average of 250
138 µmol photons m^{-2} s^{-1}. Each bottle had two pieces of tubing inserted to allow for an aeration
139 system (with humidifier) and a syringe to allow for sterile subsampling. Cells were acclimated
140 to the experimental conditions for five weeks under semi-continuous culturing, with dilutions
141 of fresh medium every five-six days (1 mL: 100 mL fresh medium), as cells reached stationary
142 phase. During the last two weeks of the acclimation period, growth rates were obtained to check
143 cells had acclimated to their respective temperatures (i.e. rates were the same over two growth
144 cycles) before growing cells for harvesting in exponential phase (day 4-5). Apart from daily
145 sampling for cell density, all subsampling was performed on the same day. All culturing was
146 conducted under sterile (laminar flow) conditions.
147
148 *Growth rate, cell size, productivity, photosynthesis and chlorophyll content*
149 Cell density was measured daily (n = 4). Aliquots of 1 mL were subsampled cleanly using a
150 sterile syringe and fixed in glutaraldehyde (1% v/v final concentration), then stored at 4 °C for

at least 1 h. Cell count and volume was determined using a particle counter (MultisizerTM 4 Coulter Counter® Beckman Coulter Inc., California, USA) with a 100 micron aperture tube. Sample volumes were diluted (1:10) with filtered seawater (0.22 μm filter) to meet instrument operational requirements (minimum analytical volume of 5 mL). Population statistics (cell density and cell size) were calculated on > 500 cells, using a size-range specific gating, and specific growth rates calculated using the difference in cell densities between days 4 and 5. The growth conditions (high light and bubbling) resulted in a very short exponential phase (< 48 h), meaning only two data points could be used for obtaining growth rates before cultures entered stationary phase or began to decline. Using only two data points could result in an underestimation of absolute growth rates, however, for the purpose of this study, it was the shape of the response to temperature as opposed to absolute rates, which was of primary interest.

Chlorophyll *a* concentration (n = 4) was determined by filtering 15 mL of culture onto GF/C filters that were then flash frozen in liquid N_2 and stored at -80 °C until analysis. Pigments were extracted in 90% acetone and incubating at 4°C in the dark for 24 h. Chlorophyll content was determined using a spectrophotometer (Cary50:Varian, Santa Clara, CA, USA) and calculated using the equations of (Jeffrey and Humphrey 1975), modified by Ritchie (2006).

Using a four-channel fiber-optic oxygen meter (Pyroscience FireSting O2, Germany) net O_2 production and respiration were measured. The custom-built system consisted of four 5.1 mL glass vials with oxygen sensor spots (Pyroscience, Germany) attached on the inside of the vials using non-toxic silicon glue (Sheehan et al. 2020). To obtain dark respiration and net photosynthesis rates, cultures were subsampled (n = 4) to fill each vial (no headspace) and then sealed. All vials were stirred continuously using cuvette stirrers to allow homogenous mixing

of gases throughout the measurement. The rack holding the vials was then placed in the tank from where the samples originated and covered to block out all light. Oxygen concentration was measured continuously and data collected every 1 s. Measurements were carried out for > 5 min (at least 300 data points per rate estimate), until the change in oxygen concentration was linear over time and the end point at least 2-3 times lower than the intrinsic noise in the optode signal (5-20 min). Following recording in the dark, the cover was removed and samples exposed to light (250 μmol photons m^{-2} s^{-1}) until the net photosynthetic rate became linear and oxygen concentration was 2-3 greater than the intrinsic noise of the optode. Respiration and photosynthesis rates were determined from the slope of the change of oxygen concentration in the vials and gross productivity calculated by summing of respiration and net production rates. From these two parameters, the photosynthesis to respiration ratio (P:R), a measure of carbon use efficiency, was determined. At the end of measurements, a 1 mL aliquot was taken from each vial and fixed with glutaraldehyde (1% v/v final concentration) to determine the cell density of the sample (using the Multisizer as described above).

Photosynthetic health of the cultures was measured using a Pulse Amplitude Modulated (PAM) fluorometer (Water- PAM; Walz GmbH, Effeltrich, Germany). For all temperatures, maximum quantum yield of PSII (F_V/F_M), a measure of maximum photochemical potential, was recorded after 10 min dark-adaptation followed by a saturating pulse of light (intensity=10, width=0.8). For determination of the effective quantum yield of PSII ($\Delta F/F_M'$), which is a measure of electron transport efficiency at growth irradiance, measurements of F' and F_M' were taken after 10-15 min exposure to average light conditions (250 μmol photons m^{-2} s^{-1}) for all temperatures. Non-photochemical quenching (NPQ), a measure of heat dissipation from the reaction centre of PSII and form of photoprotection, was calculated from the dark and light-adapted maximum fluorescence values (n = 4).

Silicification

To determine temperature specific rates of silica precipitation by *T. pseudonana*, subsamples of exponentially growing culture from the 16, 20, 24 and 28 °C treatments (n = 3) were incubated under experimental conditions for 24 h in the presence of a fluorescent probe (final concentration 0.125 µM) Lysosensor Yellow/Blue DND-160 (PDMPO, ThermoFisher Scientific, Australia) following the methods detailed by Leblanc and Hutchins (2005). Total biogenic silicate (bSi) production and active silica deposition of the culture populations were measured by filtering the incubated culture onto a 47 mm polycarbonate filter (0.6 µm; Millipore, Bayswater, Australia), which was then rinsed with filtered seawater to remove residual and unbound PDMPO. Diatom frustules were initially solubilised via a hot-alkaline-digest to release frustule-bound PDMPO before fluorometric analysis via a scanning UV-spectrofluorometer (50 Bio; Cary, Agilent Technologies, U.S.A.) set to excite at 375 nm. Samples were compared against a standard curve (R^2 = 0.995) made with 125 µM PDMPO solution that was prepared using the digestion (NaOH-HCl) matrix. Using a separate aliquot of the alkaline-digest, colorimetric analysis of reactive silicate was conducted following the methodology of Strickland and Parsons (1968) and modified by Nelson et al. (1989). Absorbance was measured at 810 nm (Cary Eclipse, Agilent Technologies, U.S.A.) and compared against a standard curve (R^2 = 0.997) made with sodium metasilicate stock solution. Data were normalised to cell density and volume that was measured following PDMPO incubation using the particle counter, as described above. By measuring both PDMPO incorporation and total bSi of the culture, we were able to determine if temperature influenced rate of newly precipitated silicate deposition into the diatom frustules.

Macromolecular composition

To determine macromolecular (protein and lipid) compositional changes with temperature, cells fixed with 2% formalin were analysed using Fourier Transform Infrared (FTIR) microspectroscopy. Spectral data were collected on the Infrared Microspectroscopy Beamline (2BMIB) at the Australian Synchrotron, Melbourne, Australia in November 2015 according to methods described previously (Petrou et al. 2018; Sheehan et al. 2020) with some modifications. Briefly, formalin fixed cells were pipetted directly onto a calcium fluoride window (0.3 mm thick) and sealed within a modified micro-compression chamber (Spectratech inc., Oak Ridge, USA; (Tobin et al. 2010) to prevent evaporation before and during measurements. Measurements were made on hydrated cells to reduce resonant mie scattering (RmieS; (Bambery et al. 2012). Spectra were acquired over the measurement range 4000-800 cm^{-1} with a Vertex 80v FTIR spectrometer (Bruker Optics, Ettlingen, Germany) in conjunction with an IR microscope (Hyperion 2000, Bruker) fitted with a mercury cadmium telluride detector cooled with liquid nitrogen. The microscope was connected to a computer-controlled microscope stage contained within a box purged with dehumidified air. Measurements were made in transmission mode at an aperture size of 5 µm x 5 µm and spectral acquisition and instrument control were performed using Opus 6.5 software (Bruker). Spectra were analysed using custom made scripts with the regions of 3050−2800 and 1770−1100 cm^{-1}, which contain the major biological bands, selected for analysis. Data were smoothed (4 points either side) and second derivative (third-order polynomial) transformed using the Savitzky-Golay algorithm from the 'prospectr' package (Stevens and Ramirez-Lopez 2013) and then normalised using the single normal variate (SNV) method. Macromolecular content for biomolecules of interest (Table 2) was determined by integrating the area under each assigned peak, providing metabolite content according to the Beer-Lambert Law that assumes a direct relationship between absorbance and analyte concentration (Wagner et al. 2010). Peak areas for each protein- or lipid-related macromolecule were compared across four temperatures to uncover

temperature-driven changes in diatom energy storage allocation, uncovering potential physiological changes in the cell and indicating biochemical shifts that may influence food web dynamics.

Data analysis

All plots and data analyses were performed in R 3.6 (R Development Core Team 2018). Phenotypic trait data (growth rates, biovolume and P:R) were tested for temperature-driven responses using a non-linear quadratic fit, while cell volume and chlorophyll *a* content were log transformed and tested for temperature-driven trends using linear regression. Fluorescence parameters, macromolecular content and silicification were analysed for statistical significance using a one-way Analysis of Variance (ANOVA) with temperature as a fixed factor and a significant level (α) < 0.05. To better understand the relationships between variables, a principle component analysis (PCA) was conducted on key functional traits for strains grown at 16, 20, 24 and 28 °C, using the ggbiplot package.

Results

Temperature-dependent growth rates of *T. pseudonana* followed an expected bell-shaped response ($R^2 = 0.59$; $F_{2,29} = 20.88$, $p < 0.0001$) across the temperature range used (14 – 28 °C) with a maximum growth rate of 4.96 ± 0.32 d^{-1} (mean ± SD) at a thermal optimum (T_{opt}) of 21.05 °C and minimum growth rates of 0.99 ± 0.1 d^{-1} at 14 °C (Fig. 1a). There was minimal change in growth rates between 16 and 24 °C, suggesting *T. pseudonana* has a broad thermal niche, however, temperatures on either side of these values resulted in a steep decline in growth rate. When compared with a thermal performance curve generated from *T. pseudonana* growth rates compiled by Kremer et al. (2017), the pattern and thermal optimum from this study was close to those of previous work, with a T_{opt} of 22 °C (Fig. 1b). Cell volume more than doubled

from 14 to 28 °C, following a linear (R^2 = 0.80; p <0.0001) increase with temperature (Fig. 2a). Chlorophyll *a* quota showed a similar response (R^2 = 0.24; p-value = 0.004), although with some deviation around the T_{opt} (Fig. 2b). A reasonable correlation (R^2 = 0.32; p < 0.0008) however, was obtained between the two parameters (Fig. 2c). The total biovolume of the culture (a product of maximum cell density and cell volume) followed a bell-shaped response (R^2 = 0.49; $F_{2,29}$ = 14.14; p <0.0001), matching growth rate data, with a maximum yield at 20.9 °C and a steep drop off in yields at 14 °C and temperatures above 24 °C (Fig. 2d).

Gross primary productivity to respiration ratio (P:R) followed a bell-shaped curve (R^2 = 0.29; $F_{2,29}$ = 5.87; p = 0.007) showed no significant change from 14 – 18 °C, but rapidly increased to values around 4:1 between 20 and 24 °C before declining again, with a T_{opt} of 21.3 °C (Fig. 3a). Interestingly, there were no clear temperature trends or changes in chlorophyll *a* fluorescence parameters (Fig. 3b), and with the exception of a dip at 18 °C, no temperature-driven differences were detected in maximum quantum yield of PSII (F_V/F_M), light-adapted effective quantum yield ($\Delta F/F_M'$) or non-photochemical quenching (NPQ). Growth rate as a function of cell volume followed a bell curve, where cells growth at T_{opt} were moderate in cell size, whereas the largest and smallest cells fell outside optimal growth conditions (Fig 3c). Growth rate as a function of carbon use efficiency (P:R) showed no clear relationship, instead suggesting a disconnect between productivity and growth at all temperatures (Fig. 3d).

Biogenic silica (bSi) per cell volume was not signifantly different between temperature treatements as a result of the high variability between measurement (Fig. 4a). However, a linear regression on all data points revealed a significant temperature-dependent relationship (R^2 = 0.39; $F_{1,10}$ = 6.36; p = 0.030), with bSi diminishing with increased temperature (Fig. 4a). Silicate deposition rate, determined by measuring the incorporation of PDMPO over time,

normalised to cell volume showed significantly higher silicification ($F_{3,8} = 19.91$; $p < 0.0004$) in cells grown at 16 °C (Fig. 4b), from an average of < 2 at 28 °C to over 6 amol PDMPO μm^{-3}. While there was a strong influence of cell size on silica content—with PDMPO incorporation rates four-fold higher at 16 °C than at 28 °C—the difference in cell size alone cannot account for the difference in PDMPO incorporation, as changes in cell volume were linear between 16 and 28 °C (Fig. 2a), whereas PDMPO per unit volume showed a non-linear response to temperature. Instead, PDMPO incorporation rate showed a distinct increase at 16 °C, with no variability amongst the warmer temperatures (Fig. 4b).

We detected temperature-related changes in cellular content of saturated lipids (2918 cm^{-1}), with 16 °C significantly lower ($F_{3,149} = 18.41$; $p < 0.005$) than all other temperatures, and 20 °C significantly lower ($p = 0.018$) than 28 °C (Fig. 5a). There was also a significant increase in saturated fatty acids (2850 cm^{-1}) with increasing temperature (Fig. 5b), where cells grown at 16 °C had significantly lower fatty acid concentrations than those grown at 24 °C and 28 °C ($F_{3,149} = 14.83$; $p \leq 0.001$), and cells grown at 20 °C had lower fatty acid content than those grown at 28 °C ($F_{3,149} = 14.83$; $p = 0.002$). The ester functional groups (related to ν(C=O) stretching from lipids and fatty acids; 1745 cm^{-1}), reached a maximum at 20 °C, with those cells having significantly higher concentrations than those grown at 16 °C ($F_{3,128} = 8.66$, $p < 0.0001$) and 28 °C ($p = 0.04$; Fig. 5c). Protein (Amide II 1540 cm^{-1}) also increased with temperature (Fig. 5d), with strains grown at 28 °C having significantly higher protein content than those grown at all other temperatures ($F_{3,143} = 12.81$; $p < 0.0001$). Similarly, the protein-related methyl groups (1460 cm^{-1}) were significantly higher in the cells grown at 28 °C ($F_{3,147} = 14.04$; $p \leq 0.0002$; Fig. 5e). The cell-specific lipid to protein ratio followed a bell shape, with a peak in lipid:protein content at 20 °C ($F_{3,121} = 7.58$; $p = 0.0001$; Fig. 6a). Despite the similar

ratios, the ratio at 16 °C was a result of lower relative concentrations of both macromolecules, whereas the lowered ratio at 28 °C was driven by a strong increase in protein content (Fig. 5).

The relationship between relative protein content and silicification (overlaid with cell volume), showed that temperature had no effect on silica content at supra-optimal temperatures (above 20 °C), whereas protein increased in both directions, i.e. in cells grown outside their temperature optimum (Fig. 6b). Importantly, as with silica content, the difference in cell size alone cannot account for the difference in protein in the cells, instead the response pattern is driven largely by temperature. Similarly, we saw an inverse temperature relationship between cell silicification and saturated fatty acid content, whereby cells at the warmest temperature had the lowest silica precipitation rates but the highest saturated fatty acid content (Fig. 6c). Combined, these data show that the cells grown in the warmest conditions were larger, richer in both lipids and proteins with reduced frustule thickness. Combining physiological and morphological trait data using principle component analysis (PCA), we see clear temperature-driven separation of *T. pseudonana* phenotypes, with PC1 explaining almost 52.3% of the variability, and PC2 explaining another 20.4% (Fig. 7). The phenotypic traits of greatest influence along PC1 were growth rate, F_V/F_M and biovolume, which were anticorrelated with Chl *a* content. PC2 was most influenced by the strong increase in PDMPO in low temperature cells followed by differences in P:R. Cell volume followed temperature, influencing both axes to some degree (Fig. 7).

Discussion

Surface ocean temperature has a fundamental influence on primary productivity, community structure and trophic interactions (Taucher and Oschlies 2011). It plays a major role in controlling the health and physiology of phytoplankton, regulating cell metabolism, cell

volume, short-term nutrient uptake and macromolecular composition (Berges et al. 2002; Marañón et al. 2013; Montagnes and Franklin 2001). Because of its strong influence on physiology, temperature is considered a main determinant of species' realised niches (Irwin et al. 2015; Irwin et al. 2012) and the principle driver underpinning phytoplankton biogeography (Longhurst 2010). As oceans become warmer however, the boundaries currently defined by species physiology will invariably begin to shift, altering the patterns and processes that currently dominate defined coastal and oceanic regions (Barton et al. 2016). Determining how phytoplankton will respond to future climate scenarios is complex but improved understanding of the phenotypic responses of diatoms to temperature will be invaluable for accurately predicting changes in community composition, productivity, biogeochemical cycling, and the health of our future oceans.

Physiological responses to temperature

Optimal growth in phytoplankton is obtained by sustaining energy balance in the cell; that is, balancing energy supply derived from photosynthesis with energy consumption via Calvin Cycle activity. Ideal conditions allow for photosynthesis to occur without biochemical or physiological modifications to the cell, whereas imbalances induced by sub-optimal conditions often result in changes to cell physiology. In this study, we determined the thermal optimum for growth of *T. pseudonana* as 21°C, consistent with previous thermal performance studies (Baker et al. 2016; Boyd et al. 2013). We confirmed a relatively broad thermal niche for *T. pseudonana*, with minimal variation in growth rates between 16 and 24 °C, indicative of its cosmopolitan distribution (Leblanc et al. 2012), but saw rapid declines in growth rate above and below these temperatures, identifying thermal thresholds for physiological homeostasis. The relatively high growth rates in this study (1-5 d^{-1}) were a result of the growth conditions of high light levels (average ~250 µmol photons m^{-2} s^{-1}) and constant air bubbling, which

375 enhance microalgal growth due to greater mass-transfer of CO_2 and a more uniform light-field
376 (Ugwu and Aoyagi 2012) as a result of stirring.
377
378 The influence of temperature on photosynthesis is caused by complex kinetics of the enzyme
379 Ribulose-1,5-bisphosphate carboxylase/oxygenase (RuBisCo). RuBisCo catalyses the first step
380 in two competing pathways; photosynthetic carbon assimilation (via carboxylase activity) and
381 photorespiration (via oxygenase activity). In *T. pseudonana,* photosynthetic performance,
382 measured as P:R, peaked at a similar temperature (21.3°C) to growth optimum, and as with
383 growth rates, dropped off rapidly with both warmer and cooler temperatures. These data would
384 suggest that the temperatures just above T_{opt} enhanced carboxylase performance in *T.*
385 *pseudonana*, a response that has been shown to occur with increasing temperatures up to 30 °C
386 (Salvucci and Crafts-Brandner 2004), after which CO_2 affinity for RuBisCo declines, limiting
387 photosynthesis. The decrease in P:R above 24 °C in this study, was driven by higher respiration
388 rates. Higher temperatures are known to enhance respiration, reducing overall carbon use
389 efficiency, and thus overall productivity (Padfield et al. 2016). At the other end of the bell
390 curve, sub-optimal temperatures, such as the lowest temperature tested in this study (14 °C),
391 likely inhibited carboxylase activity in *T. pseudonana* and therefore lowered photosynthetic
392 energy production and slowed growth.
393
394 Congruent with previous work we found a positive relationship between temperature and
395 chlorophyll *a* content (Baker et al. 2016; Berges et al. 2002; Liang et al. 2019), which can be
396 attributed to the temperature sensitive kinetics of carboxylase activity. Under cold conditions,
397 temperature-dependent dark reaction rates slow, which means that less light is needed to
398 saturate the photosystem that is operating at a reduced capacity (Ras et al. 2013). If no cellular
399 adjustments are made, oversupply of energy production via photosynthesis (light reactions) can

lead to photoinhibition. Therefore, microalgae reduce their light-harvesting pigment content (Chl *a*), avoiding over-excitation of the photosystem and preventing damage (Geider 1987). This low-temperature chlorosis is a common adaptive response by microalgae to ameliorate photodamage when light levels remain consistent while temperatures drop (Geider 1987), as was the case in this study. The lack of adjustment in photosynthetic electron transport and non-photochemical quenching with temperature suggests that the reduction in chl *a* content was effective for avoiding photoinhibition in the low temperature cells.

Morphological responses to temperature

Size is a key phenotypic trait in phytoplankton, influencing the structure and functioning of pelagic food webs and determining the fate of organic carbon (Finkel et al. 2009; Sommer et al. 2016). Here we measured an increase in cell volume with temperature, consistent with previous temperature studies on *T. pseudonana* (Baker et al. 2016; Berges et al. 2002). The reason for temperature-induced cell enlargement is uncertain, potentially stemming from the slowing down of cell division, thereby allowing for larger cells to develop, or perhaps it is that cell size is a direct physiological response to warming and the high energetic cost of maintaining a large cell volume reduced the energy available for growth (Sommer et al. 2016). There is a similar lack of explanation for the significant shrinking of *T. pseudonana* cells with cooling. Given that division rates were not enhanced by lowered temperatures, no argument can be made for this resulting in smaller cell size.

Total cell abundance if often considered the ultimate 'ecological currency' (Li et al. 2006), but in the context of ocean biogeochemistry or fisheries resources, productivity or biomass can have equal importance. We found total biomass (measured as biovolume) of the cultures peaked around the thermal optimum, indicating that differences in cell abundance because of

differences in growth rate were independent of the doubling in cell volume, voiding the idea that the additional biomass of larger cells might account for losses in cell number. Populations achieve maximum density once all available resources are spent. As such, yields can be enhanced only by an increase in available resources or by a decrease in resource use by individuals (DeLong and Hanson 2011). In our study, resource availability was fixed (with no additional nutrient input during the growth cycle), which implies that declines in maximum cell density at warmer temperatures could be due to increased resource demand via the kinetic effect of temperature on metabolic rates (Brown et al. 2004; Regaudie-de-Gioux and Duarte 2012). Effectively, the *T. pseudonana* cells grown at higher temperatures may have experienced a trade-off, where larger body size and possibly greater resource requirement, resulted in reduced P:R and growth efficiency. If we consider predicted nutrient limitation that is expected to occur with shoaling of surface waters under warming conditions (Bopp et al. 2001), it can be supposed that larger cells will undergo even slower growth, as demand for nutrients will more rapidly outstrips supply. In contrast, at lower temperatures slow division rates due to temperature constraints on enzymatic reactions, combined with smaller cells account for the low biomass yields. This would reduce nutrient demand and the resulting higher SA:V ratio would further ameliorate any potential nutrient limitation.

One macronutrient uniquely essential for diatoms is silicon (Martin-Jezequel et al. 2000), which is used in frustule formation and is thus intimately linked with diatom cell growth and division (Darley and Volcani 1969; Martin-Jezequel et al. 2000). The strong increase in silicification of cells grown at cooler temperatures is consistent with previous work (Baker et al. 2016) and suggests a thermal constraint on silica uptake rates, polymerisation processes or frustule deposition. Previous work has shown growth rate to be anticorrelated with frustule thickness (Martin-Jezequel et al. 2000). Our data however, show a bell curve response for

450 growth rate and a clear non-linear response in silicification, with a sharp increase in silica
451 incorporation as temperature is lowered to 16 °C, suggesting a thermal threshold at which
452 silicification diminishes independent of cell division. It was recently shown that acidification
453 of seawater diminished silicification in some cold-water diatoms (Petrou et al. 2019), and the
454 present data suggests that warmer temperatures may elicit a similar effect. If so, with the
455 combined expected changes to ocean temperature and pH, diatoms may experience compound
456 effects on silicification processes. Given that this process is fundamental to diatom growth and
457 biogeochemical cycling, further research in the context of climate change related ecological
458 shifts are needed.
459
460 *Biochemical responses to temperature*
461 Diatom growth requires the uptake of nutrients and their conversion into biomass to form new
462 cells. The rate of these biochemical processes is influenced by temperature, via its regulation
463 on cell metabolism (Berges et al. 2002; Regaudie-de-Gioux and Duarte 2012). Biochemical
464 responses of diatoms to temperature have been shown to be species specific (Sackett et al.
465 2014), with marine microalgae shown to favour saturated fatty acid biosynthesis under both
466 warmer conditions (Renaud et al. 2002) and cooler conditions (Converti et al. 2009). In this
467 study, increased temperature caused an increase in relative saturated lipid and fatty acid
468 content. We also saw an increase in protein with warming, congruent with changes seen in a
469 low temperature adapted strain (16 °C) of *T. pseudonana* following a six degree increase in
470 growth temperature(Liang et al. 2019). Given our strain was adapted to 20 °C, the increase in
471 protein content detected at 28 °C closely reflects the response observed previously (Liang et
472 al. 2019). While changes in lipid and protein content can have a profound effect at the level of
473 an individual cell, alteration in their availability can impact food web structure and health
474 (Bhavya et al. 2019; Jo et al. 2017; Laws 1991; Lindqvist and Lignell 1997). Proteins have a

475 higher carbon transfer efficiency to herbivores than other macromolecules (Lindqvist and
476 Lignell 1997), whereas lipids present the highest caloric value and are generally synthesised as
477 energy reservoirs (Bhavya et al. 2019), therefore increased concentrations in cells grown at
478 warmer temperatures could mean greater nutrient availability for higher trophic organisms. It
479 is important to mention that in this study, cells were also larger at warmer temperatures, and
480 therefore it is tempting to suggest that differences in relative macromolecular content were a
481 result of differences in cell size. However, in diatoms, the chemical composition of the cell has
482 been shown to be largely independent of cell size, as diatoms increase their cell size
483 predominantly via increasing the size of their central vacuole (Finkel et al. 2016; Finkel et al.
484 2004) and as such, differences in relative nutritional value can be considered as largely
485 independent of changes in size.
486
487 *Ecological and biogeochemical consequences*
488 Considering ecological consequences of our observed phenotypic responses, substantial
489 structural and functional changes to pelagic food webs may ensue if our data are representative
490 of diatoms in general. If we assume that a higher lipid:protein ratio is beneficial to zooplankton
491 and other grazers, then cells grown at T_{opt} would provide the best resource. However, if protein
492 rich cells are favoured, then *T. pseudonana* grown at higher temperatures would be preferred.
493 Grazing rates too are important considerations, as they are a function of cell size (Sommer et
494 al. 2016). Larger cells may provide more food, but may also cause shifts in predator populations
495 toward more generalist feeders and those able to graze on larger cells (Sommer et al. 2016).
496 Similarly, we need to consider the role of changes to silicification, which were reduced at
497 higher temperatures. Silica frustules act as mechanical protection against grazing; the thicker
498 the frustule the harder to digest (Hamm et al. 2003). The decline in silica incorporated by *T.*
499 *pseudonana* at warmer temperatures indicates thinner frustules that could be more easily

digested, possibly resulting in increased grazing. There is, however, yet another potential effect to consider; with reduced silica deposition, vegetative cells may have difficulty in dividing, potentially causing diatom cells to enter a senescent stage of growth (Martin-Jezequel et al. 2000). This in turn could lower secondary productivity and cause a decline in grazer reproductive success.

If we consider these observed phenotypic changes in the context of future biogeochemistry, where warmer oceans lead to fewer, larger diatoms with lower silica content, consequences for carbon and silica export are evident. As the primary siliceous organism responsible for the production of biogenic silica in open ocean and coastal zones, the decline in both cell numbers and amount of silica per cell will mean less silica produced and ultimately exported (Tréguer and De La Rocha 2013). Similarly, larger cells contain less carbon per unit biovolume, a trait especially pronounced in diatoms because of cell vacuolation (Sommer et al. 2016), and thus fewer, larger diatoms may also reduce carbon export. The direct effect of these morphological changes on the diatoms ballast however, is unknown. The sinking velocity of phytoplankton is heavily dependent on cell size (Sommer et al. 2016), so the larger cells at warmer temperatures may be considered better sinkers, however, the four-fold difference in silicification may mean that the decreased frustule density at warmer temperatures may counter any gains via increased cell volume. Furthermore, *T. pseudonana* grown at warmer temperatures had more lipids, which are less dense than seawater, and combined with the knowledge that diatoms predominantly increase their size by increasing vacuolation (Finkel et al. 2016), it is fair to assume that ballast will be overall reduced. If so, combined with lower cell numbers and potentially higher grazing rates, we might anticipate more nutrient remineralisation in surface waters and an overall reduction in carbon and silica export to the ocean interior. This could be further exacerbated by nutrient limitation, due to projected increased ocean shoaling (Bopp et

al. 2001), whereby the larger cells, having higher nutrient requirements (Finkel et al. 2004), will be further challenged, and ultimately could result in localised extinction due to competition from smaller species.

Conclusion

Temperature plays an important role in the biological functioning of diatoms, which are integral to the biological pump and global biogeochemical cycling of carbon and silica. As temperatures continue to increase, it is important to understand how these environmental changes will impact diatoms and subsequent flow-on effects. This study investigated the changes in physiological characteristics, silicate deposition and macromolecular composition of model diatom species *T. pseudonana* in response to temperature. Based on the results herein, an increase in water temperature under future climate will bring forth fewer, but larger diatoms that are less productive, less silicified, but with higher lipid and protein content. Metabolically, these cells are expensive to run, with higher respiration rates and nutrient requirements. Ecologically, these larger, less silicified cells are more easily grazed and potentially a favourable energy source. Biogeochemically, reduced ballast in a warmer ocean has potentially severe implications for carbon and silica export. These broad ecological consequences derived from the observations presented, must be tempered by the fact that only one species was examined and we recognise that these effects will likely vary between species. Similarly, temperature was tested in the absence of other variables, thereby excluding interactive influences. Despite their limitations, temperature experiments on individual species constitute a fundamental component to building a better understanding of the impending effects of climate change on diatoms.

Author contributions: KP designed the experiment; all authors conducted the experiment; sample and data collection CES, KGB, KP; formal data analysis and visualisation DAN; writing of first draft KP; all authors contributed to and approved the final draft of the manuscript.

Acknowledgements: We thank Australian Synchrotron Beamline Scientists Drs Mark Tobin and Jitraporn Vongsvivut for technical support in synchrotron IR microspectroscopy data acquisition. Part of this work was funded by the Australian Synchrotron through merit based beamtime awarded on the Infrared Microscopy (IRM) beamline (AS153/IRM/10005) awarded to KP. CES and KGB were supported by funding provided by the Climate Change Cluster and the School of Life Science at the University of Technology Sydney.

References:

Baker, K. G., C. M. Robinson, D. T. Radford, A. S. McInnes, C. Evenhuis & M. A. Doblin, 2016. Thermal Performance Curves of Functional Traits Aid Understanding of Thermally Induced Changes in Diatom-Mediated Biogeochemical Fluxes. Frontiers in Marine Science 3(44) doi:10.3389/fmars.2016.00044.

Bambery, K. R., B. R. Wood & D. McNaughton, 2012. Resonant Mie scattering (RMieS) correction applied to FTIR images of biological tissue samples. Analyst 137(1):126-132 doi:10.1039/C1AN15628D.

Barton, A. D., A. J. Irwin, Z. V. Finkel & C. A. Stock, 2016. Anthropogenic climate change drives shift and shuffle in North Atlantic phytoplankton communities. Proceedings of the National Academy of Sciences 113(11):2964 doi:10.1073/pnas.1519080113.

573 Berges, J. A., D. E. Varela & P. J. Harrison, 2002. Effects of temperature on growth rate, cell
574 composition and nitrogen metabolism in the marine diatom Thalassiosira pseudonana
575 (Bacillariophyceae). Marine Ecology Progress Series 225:139-146.
576 Bhavya, P., B. K. Kim, N. Jo, K. Kim, J. J. Kang, J. H. Lee, D. Lee, J. H. Lee, H. Joo & S. H.
577 Ahn, 2019. A review on the macromolecular compositions of phytoplankton and the
578 implications for aquatic biogeochemistry. Ocean Science Journal 54(1):1-14.
579 Bopp, L., P. Monfray, O. Aumont, J. Dufresne, H. Le Treut, G. Madec, L. Terray & J. Orr,
580 2001. Potential impact of climate change on marine export production. Global
581 Biogeochemical Cycles 15(1):81-99.
582 Boyd, P. W., T. A. Rynearson, E. A. Armstrong, F. Fu, K. Hayashi, Z. Hu, D. A. Hutchins, R.
583 M. Kudela, E. Litchman, M. R. Mulholland, U. Passow, R. F. Strzepek, K. A.
584 Whittaker, E. Yu & M. K. Thomas, 2013. Marine Phytoplankton Temperature versus
585 Growth Responses from Polar to Tropical Waters – Outcome of a Scientific
586 Community-Wide Study. PLOS ONE 8(5):e63091 doi:10.1371/journal.pone.0063091.
587 Brown, J. H., J. F. Gillooly, A. P. Allen, V. M. Savage & G. B. West, 2004. Toward a metabolic
588 theory of ecology. Ecology 85(7):1771-1789 doi:10.1890/03-9000.
589 Brown, M. R., 2002. Nutritional value and use of microalgae in aquaculture. Avances en
590 Nutrición Acuicola.
591 Burrows, M. T., D. S. Schoeman, A. J. Richardson, J. G. Molinos, A. Hoffmann, L. B. Buckley,
592 P. J. Moore, C. J. Brown, J. F. Bruno, C. M. Duarte, B. S. Halpern, O. Hoegh-Guldberg,
593 C. V. Kappel, W. Kiessling, M. I. O'Connor, J. M. Pandolfi, C. Parmesan, W. J.
594 Sydeman, S. Ferrier, K. J. Williams & E. S. Poloczanska, 2014. Geographical limits to
595 species-range shifts are suggested by climate velocity. Nature 507(7493):492-495
596 doi:10.1038/nature12976.

597 Converti, A., A. A. Casazza, E. Y. Ortiz, P. Perego & M. Del Borghi, 2009. Effect of
598 temperature and nitrogen concentration on the growth and lipid content of
599 Nannochloropsis oculata and Chlorella vulgaris for biodiesel production. Chemical
600 Engineering and Processing: Process Intensification 48(6):1146-1151.
601 Darley, W. M. & B. Volcani, 1969. Role of silicon in diatom metabolism: a silicon requirement
602 for deoxyribonucleic acid synthesis in the diatom Cylindrotheca fusiformis Reimann
603 and Lewin. Experimental Cell Research 58(2-3):334-342.
604 DeLong, J. P. & D. T. Hanson, 2011. Warming alters density dependence, energetic fluxes,
605 and population size in a model algae. Ecological Complexity 8(4):320-325
606 doi:https://doi.org/10.1016/j.ecocom.2011.07.001.
607 Edwards, M. & A. J. Richardson, 2004. Impact of climate change on marine pelagic phenology
608 and trophic mismatch. Nature 430(7002):881-884.
609 Falkowski, P. G., R. T. Barber & V. Smetacek, 1998. Biogeochemical Controls and Feedbacks
610 on Ocean Primary Production
611 10.1126/science.281.5374.200. Science 281(5374):200-206.
612 Finkel, Z., M. Follows & A. Irwin, 2016. Size-scaling of macromolecules and chemical energy
613 content in the eukaryotic microalgae. Journal of Plankton Research 38(5):1151-1162.
614 Finkel, Z. V., J. Beardall, K. J. Flynn, A. Quigg, T. A. V. Rees & J. A. Raven, 2009.
615 Phytoplankton in a changing world: cell size and elemental stoichiometry. Journal of
616 Plankton Research 32(1):119-137 doi:10.1093/plankt/fbp098.
617 Finkel, Z. V., A. J. Irwin & O. Schofield, 2004. Resource limitation alters the 3/4 size scaling
618 of metabolic rates in phytoplankton. Marine Ecology Progress Series 273:269-279.
619 Gao, K., E. W. Helbling, D. Hader & D. Hutchins, 2012. Responses of marine primary
620 producers to interactions between ocean acidification, solar radiation, and warming.
621 Marine Ecology Progress Series 470:167-189

622 Gattuso, J.-P., A. Magnan, R. Billé, W. W. Cheung, E. L. Howes, F. Joos, D. Allemand, L.
623 Bopp, S. R. Cooley & C. M. Eakin, 2015. Contrasting futures for ocean and society
624 from different anthropogenic CO2 emissions scenarios. Science 349(6243):aac4722.
625 Geider, R., 1987. Light and temperature dependence of the carbon to chlorophyll *a* ratio in
626 microalgae and cyanobacteria: Implications for physiology and growth of
627 phytoplankton. The New Phytologist 106:1-34.
628 Giordano, M., J. Beardall & J. A. Raven, 2005. CO2 concentrating mechanisms in algae:
629 Mechanisms, Environmental Modulation, and Evolution. Annual Review of Plant
630 Biology 56(1):99-131 doi:doi:10.1146/annurev.arplant.56.032604.144052.
631 Giordano, M., M. Kansiz, P. Heraud, J. Beardall, B. Wood & D. McNaughton, 2001. Fourier
632 transform infrared spectroscopy as a novel tool to investigate changes in intracellular
633 macromolecular pools in the marine microalgal *Chaetoceros muellerii*
634 (Bacillariophyceae) Journal of Phycology 37(2):271-279 doi:10.1046/j.1529-
635 8817.2001.037002271.x.
636 Guillard, R. R. & J. H. Ryther, 1962. Studies of marine planktonic diatoms I. *Cyclotella nana*
637 Hudstedt and *Detonula confervacea* Cleve. . Canadian Journal of Microbiology 8:229-
638 239.
639 Hamm, C. E., R. Merkel, O. Springer, P. Jurkojc, C. Maier, K. Prechtel & V. Smetacek, 2003.
640 Architecture and material properties of diatom shells provide effective mechanical
641 protection. Nature 421(6925):841.
642 Huertas, I. E., M. Rouco, V. Lopez-Rodas & E. Costas, 2011. Warming will affect
643 phytoplankton differently: evidence through a mechanistic approach. Proceedings of
644 the Royal Society B: Biological Sciences 278(1724):3534-3543.

645 Irwin, A. J., Z. V. Finkel, F. E. Müller-Karger & L. T. Ghinaglia, 2015. Phytoplankton adapt
646 to changing ocean environments. Proceedings of the National Academy of Sciences
647 112(18):5762-5766.
648 Irwin, A. J., A. M. Nelles & Z. V. Finkel, 2012. Phytoplankton niches estimated from field
649 data. Limnology and Oceanography 57(3):787-797.
650 Jeffrey, S. W. & G. F. Humphrey, 1975. New spectrophotometric equations for determining
651 chlorophyll *a, b, c1,* and *c2* in higher plants and natural phytoplankton. . Biochem
652 Physiol Pfl 165:191-194.
653 Jo, N., J. J. Kang, W. G. Park, B. R. Lee, M. S. Yun, J. H. Lee, S. M. Kim, D. Lee, H. Joo & J.
654 H. Lee, 2017. Seasonal variation in the biochemical compositions of phytoplankton and
655 zooplankton communities in the southwestern East/Japan Sea. Deep Sea Research Part
656 II: Topical Studies in Oceanography 143:82-90.
657 Juneja, A., R. M. Ceballos & G. S. Murthy, 2013. Effects of environmental factors and nutrient
658 availability on the biochemical composition of algae for biofuels production: a review.
659 Energies 6(9):4607-4638.
660 Kremer, C. T., M. K. Thomas & E. Litchman, 2017. Temperature-and size-scaling of
661 phytoplankton population growth rates: Reconciling the Eppley curve and the
662 metabolic theory of ecology. Limnology and oceanography 62(4):1658-1670.
663 Laws, E. A., 1991. Photosynthetic quotients, new production and net community production in
664 the open ocean. Deep Sea Research Part A Oceanographic Research Papers 38(1):143-
665 167.
666 Leblanc, K., J. Arístegui, E. Kopczynska, H. Marshall, J. Peloquin, S. Piontkovski, A. Poulton,
667 B. Quéguiner, R. Schiebel & R. Shipe, 2012. A global diatom database–abundance,
668 biovolume and biomass in the world ocean.

669 Li, W. K., W. Glen Harrison & E. J. Head, 2006. Coherent assembly of phytoplankton
670 communities in diverse temperate ocean ecosystems. Proceedings of the Royal Society
671 B: Biological Sciences 273(1596):1953-1960.
672 Liang, Y., J. A. Koester, J. D. Liefer, A. J. Irwin & Z. V. Finkel, 2019. Molecular mechanisms
673 of temperature acclimation and adaptation in marine diatoms. The ISME Journal
674 13(10):2415-2425 doi:10.1038/s41396-019-0441-9.
675 Lindqvist, K. & R. Lignell, 1997. Intracellular partitioning of 14CO2 in phytoplankton during
676 a growth season in the northern Baltic. Marine Ecology Progress Series 152:41-50.
677 Longhurst, A. R., 2010. Ecological geography of the sea. Elsevier.
678 Marañón, E., P. Cermeño, D. C. López-Sandoval, T. Rodríguez-Ramos, C. Sobrino, M. Huete-
679 Ortega, J. M. Blanco & J. Rodríguez, 2013. Unimodal size scaling of phytoplankton
680 growth and the size dependence of nutrient uptake and use. Ecology letters 16(3):371-
681 379.
682 Martin-Jezequel, V., M. Hildebrand & M. A. Brzezinski, 2000. Silicon metabolism in diatoms:
683 implications for growth. Journal of Phycology 36(5):821-840.
684 Mathur, S., D. Agrawal & A. Jajoo, 2014. Photosynthesis: response to high temperature stress.
685 Journal of Photochemistry and Photobiology B: Biology 137:116-126.
686 Meehl, G. A., T. F. Stocker, W. D. Collins, P. Friedlingstein, A. T. Gaye, J. M. Gregory, A.
687 Kitoh, R. Knutti, J. M. Murphy & A. Noda, 2007. Global climate projections. Climate
688 change 2007: the physical science basis. Contribution of Working Group I to the Fourth
689 Assessment Report of the Intergovernmental Panel on Climate Change. Cambridge:
690 Cambridge University Press.
691 Montagnes, D. J. S. & D. J. Franklin, 2001. Effect of Temperature on Diatom Volume, Growth
692 Rate, and Carbon and Nitrogen Content: Reconsidering Some Paradigms. Limnology
693 and Oceanography 46(8):2008-2018.

694 Murdock, J. N. & D. L. Wetzel, 2009. FT-IR microspectroscopy enhances biological and
695 ecological analysis of algae. Applied Spectroscopy Reviews 44(4):335-361.
696 Nelson, D. M., W. O. Smith, R. D. Muench, L. I. Gordon, C. W. Sullivan & D. M. Husby,
697 1989. Particulate matter and nutrient distributions in the ice-edge zone of the Weddell
698 Sea: relationship to hydrography during late summer. Deep Sea Research Part A
699 Oceanographic Research Papers 36(2):191-209 doi:https://doi.org/10.1016/0198-
700 0149(89)90133-7.
701 Padfield, D., G. Yvon-Durocher, A. Buckling, S. Jennings & G. Yvon-Durocher, 2016. Rapid
702 evolution of metabolic traits explains thermal adaptation in phytoplankton. Ecology
703 Letters 19(2):133-142.
704 Petrou, K., K. G. Baker, D. A. Nielsen, A. M. Hancock, K. G. Schulz & A. T. Davidson, 2019.
705 Acidification diminishes diatom silica production in the Southern Ocean. Nature
706 Climate Change 9(10):781-796 doi:10.1038/s41558-019-0557-y.
707 Petrou, K., D. A. Nielsen & P. Heraud, 2018. Single-Cell Biomolecular Analysis of Coral Algal
708 Symbionts Reveals Opposing Metabolic Responses to Heat Stress and Expulsion.
709 Frontiers in Marine Science 5(110) doi:10.3389/fmars.2018.00110.
710 R Development Core Team, 2018. R: A language and environment for statistical computing.
711 In: R Foundation for Statistical Computing. Retrieved from https://www.R-project.org/.
712 https://www.R-project.org/ 2019.
713 Ras, M., J.-P. Steyer & O. Bernard, 2013. Temperature effect on microalgae: a crucial factor
714 for outdoor production. Reviews in Environmental Science and Bio/Technology
715 12(2):153-164 doi:10.1007/s11157-013-9310-6.
716 Raven, J. & A. Waite, 2004. The evolution of silicification in diatoms: inescapable sinking and
717 sinking as escape? New phytologist 162(1):45-61.

718 Regaudie-de-Gioux, A. & C. M. Duarte, 2012. Temperature dependence of planktonic
719 metabolism in the ocean. Global Biogeochemical Cycles 26(1)
720 doi:10.1029/2010gb003907.
721 Renaud, S. M., L.-V. Thinh, G. Lambrinidis & D. L. Parry, 2002. Effect of temperature on
722 growth, chemical composition and fatty acid composition of tropical Australian
723 microalgae grown in batch cultures. Aquaculture 211(1):195-214
724 doi:https://doi.org/10.1016/S0044-8486(01)00875-4.
725 Ritchie, R., 2006. Consistent Sets of Spectrophotometric Chlorophyll Equations for Acetone,
726 Methanol and Ethanol Solvents. Photosynthesis Research 89(1):27-41.
727 Sackett, O., L. Armand, J. Beardall, R. Hill, M. Doblin, C. Connelly, J. Howes, B. Stuart, P.
728 Ralph & P. Heraud, 2014. Taxon-specific responses of Southern Ocean diatoms to Fe
729 enrichment revealed by synchrotron radiation FTIR microspectroscopy.
730 Biogeosciences 11(20):5795-5808.
731 Salvucci, M. E. & S. J. Crafts-Brandner, 2004. Relationship between the Heat Tolerance of
732 Photosynthesis and the Thermal Stability of Rubisco Activase in Plants from
733 Contrasting Thermal Environments. Plant Physiology 134(4):1460
734 doi:10.1104/pp.103.038323.
735 Salvucci, M. E. & S. J. Crafts-Brandner, 2004. Inhibition of photosynthesis by heat stress: the
736 activation state of Rubisco as a limiting factor in photosynthesis. Physiologia plantarum
737 120(2):179-186.
738 Sheehan, C. E., D. A. Nielsen & K. Petrou, 2020. Macromolecular composition, productivity
739 and dimethylsulfoniopropionate in Antarctic pelagic and sympagic microalgal
740 communities. Marine Ecology Progress Series 640:45-61.

741 Sommer, U., E. Charalampous, S. Genitsaris & M. Moustaka-Gouni, 2016. Benefits, costs and
742 taxonomic distribution of marine phytoplankton body size. Journal of Plankton
743 Research 39(3):494-508
744 Stevens, A. & L. Ramirez-Lopez, 2013. An introduction to the prospectr package. In: R
745 package Vignette R package version 013.
746 Strickland, J. & T. Parsons, 1968. Bull. Fish. Res. Bd Can. A practical handbook of seawater
747 analysis(167):311.
748 Suzuki, Y. & M. Takahashi, 1995. Growth responses of several diatom species isolated from
749 various environments to temperature. Journal of Phycology 31(6):880-888.
750 Taucher, J. & A. Oschlies, 2011. Can we predict the direction of marine primary production
751 change under global warming? Geophysical Research Letters 38(2).
752 Thompson, P. A., M. x. Guo & P. J. Harrison, 1992. Effects of variation in temperature. I. On
753 the biochemical composition of eight species of marine phytoplankton 1. Journal of
754 Phycology 28(4):481-488.
755 Tobin, M. J., L. Puskar, R. L. Barber, E. C. Harvey, P. Heraud, B. R. Wood, K. R. Bambery,
756 C. T. Dillon & K. L. Munro, 2010. FTIR spectroscopy of single live cells in aqueous
757 media by synchrotron IR microscopy using microfabricated sample holders.
758 Vibrational spectroscopy 53(1):34-38.
759 Tréguer, P., C. Bowler, B. Moriceau, S. Dutkiewicz, M. Gehlen, O. Aumont, L. Bittner, R.
760 Dugdale, Z. Finkel & D. Iudicone, 2018. Influence of diatom diversity on the ocean
761 biological carbon pump. Nature Geoscience 11(1):27.
762 Treguer, P., D. M. Nelson, A. J. Van Bennekom, D. J. DeMaster, A. Leynaert & B. Queguiner,
763 1995. The Silica Balance in the World Ocean: A Reestimate, Science 268(5209):375-
764 379.

765 Tréguer, P. J. & C. L. De La Rocha, 2013. The world ocean silica cycle. Annual review of
766 marine science 5:477-501.
767 Twining, B. S., S. B. Baines, S. Vogt & M. D. de JONGE, 2008. Exploring Ocean
768 Biogeochemistry by Single-Cell Microprobe Analysis of Protist Elemental
769 Composition 1. Journal of Eukaryotic Microbiology 55(3):151-162.
770 Ugwu, C. U. & H. Aoyagi, 2012. Microalgal culture systems: an insight into their designs,
771 operation and applications. Biotechnology 11(3):127.
772 Van Donk, E., A. Ianora & M. Vos, 2011. Induced defences in marine and freshwater
773 phytoplankton: a review. Hydrobiologia 668(1):3-19.
774 Vongsvivut, J., P. Heraud, W. Zhang, J. A. Kralovec, D. McNaughton & C. J. Barrow, 2012.
775 Quantitative determination of fatty acid compositions in micro-encapsulated fish-oil
776 supplements using Fourier transform infrared (FTIR) spectroscopy. Food Chemistry
777 135(2):603-609 doi:http://doi.org/10.1016/j.foodchem.2012.05.012.
778 Wagner, H., Z. Liu, U. Langner, K. Stehfest & C. Wilhelm, 2010. The use of FTIR
779 spectroscopy to assess quantitative changes in the biochemical composition of
780 microalgae. Journal of Biophotonics 3(8-9):557-566 doi:10.1002/jbio.201000019.
781
782
783

784 **Table 1** Mean temperature ± standard deviation (SD) for each temperature treatment. Data
785 based on monitoring every 5 min throughout acclimation and experimental period using
786 submersible temperature sensors.

Target temperature	Mean temperature	SD
14	13.73	0.36
16	15.68	0.52
18	18.01	0.78
20	19.85	0.42
22	22.47	0.64
24	24.33	0.60
26	26.23	0.26
28	27.99	0.10

787
788
789
790
791

792 **Table 2** Infrared band assignments of IR spectra for *T. pseudonana*

Wavenumber (cm^{-1})	Biochemical assignment	Reference
~2917	ν_{as}(C–H) from methylene (–CH_2), from saturated fatty acids	(Vongsvivut et al. 2012)
~2850	ν_{s}(C–H) from methylene (–CH_2), from saturated fatty acids	(Vongsvivut et al. 2012)
~1745	ν(C=O) of ester functional groups, from membrane lipids and fatty acids	(Murdock and Wetzel 2009; Vongsvivut et al. 2012)
~1544	δ(N–H) associated with proteins (amide II band)	(Giordano et al. 2001)
~1460	δ_{as}(CH_3) and δ_{as}(CH_2) of proteins (carboxylic group)	(Giordano et al. 2005; Murdock and Wetzel 2009)

793 νas = asymmetrical stretch; νs = symmetrical stretch; δ_{as} = asymmetrical deformation (bend); δ_{s} = symmetrical

794 deformation (bend).

795

796

Figure 1 Growth rates of *T.pseudonana* in response to temperature. **A)** Specific growth rates (per day^{-1}), **B)** Specific growth rates of multiple strains of *T. pseudonana* from numerous studies, based on data collated by Kremer et al. (2017). Data represent individual measurements (n = 4), dark grey lines show the curve fit and light grey shading shows 95% confidence intervals.

Figure 2 Physiological and morphological trait responses to temperature. **A)** cell volume (µm^3), **B)** chlorophyll *a* content (fg/cell), **C)** relationship between chl *a* and cell volume and **D)** total culture biomass (mm^3), calculated as the product of culture yield at the end of exponential growth (cells/mL) and cell volume (µm^3). Data are individual measurements (n = 4), dark grey lines are linear regressions and light grey shading represents the 95% confidence intervals. Note: y-axes are plotted on a log10 scale for plots A and B, and log10 scale of x and y-axes for plot C.

Figure 3 Productivity and photophysiological response of *T. pseudonana* to temperature. **A)** Gross productivity to respiration ratio (P:R) and respiration rate (red triangles), data are individual measurements (n = 4), grey line shows the curve fit and shaded area represent 95% confidence intervals. **B)** Chlorophyll *a* fluorescence parameters maximum quantum yield of PSII (F_V/F_M), effective quantum yield ($\Delta F/F_M'$) and non-photochemical quenching (NPQ), data represent mean ± standard error (se) (n=4). **C**) Growth rate as a function of cell volume and **D**) Growth rate as a function of P:R, data are individual measurements (n = 4).

Figure 4 Silica production and active incorporation. **A)** Biogenic silica (bSi) normalised to cell volume (fmol µm^{-3}), data show the mean ± se (n = 4), grey line shows the regression and shaded

821 area represent 95% confidence intervals and **B)** PDMPO incorporation rate (amol μm^{-3}, d^{-1}) in
822 *T.pseudonana* grown at 16, 20, 24 and 28 °C. Data represent mean values ± se (*n*=3).
823
824 **Figure 5** FTIR analysis of *T. pseudonana* grown at 16, 20, 24 and 28 °C.
825 Integrated peak areas for saturated lipids, saturated fatty acids, ester carbonyl of lipids, amide
826 II (protein) and protein-related methyl groups. Boxplots show the range of data, the 1st and 3rd
827 quartile (box) and median (black horizontal line), with black dots as outliers. The subscript
828 numbers at the bottom of the figure indicate cell replication (*n*) from 3-5 biological replicates.
829
830 **Figure 6** Relationships between lipids, proteins and silica content in *T. pseudonana* grown at
831 16, 20, 24 and 28 °C. **A)** Lipid:Protein, where the boxplot shows the range of data, the 1st and
832 3rd quartile (box) and median (black horizontal line), with black dots as outliers. The subscript
833 numbers at the bottom of the figure indicate replication (*n*). **B)** relationship between protein
834 (amide II) and PDMPO incorporation and **C)** saturated fatty acids and PDMPO incorporation.
835 In B and C, size of dot indicates mean cell volume, and colour indicates growth temperature.
836 Data represent mean values ± se (*n* = 3).
837
838 **Figure 7** Principle component analysis (PCA) with vectors of physiological and morphological
839 traits (growth rate, cell volume, chl *a*, biovolume, F_V/F_M, P:R, silicification) measured in *T.*
840 *pseudonana* grown at 16, 20, 24 and 28 °C. Size of the dot indicates mean cell volume, colour
841 indicates growth temperature (*n* = 3).
842
843
844
845

Figures:

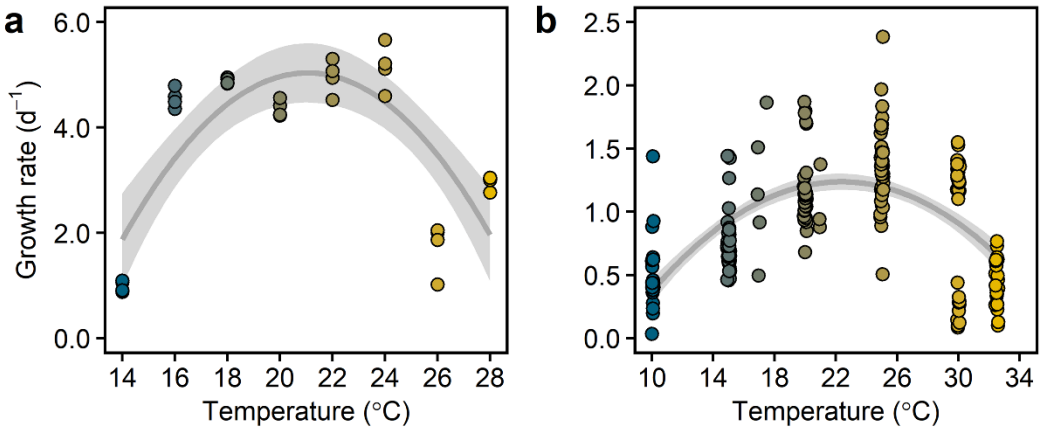

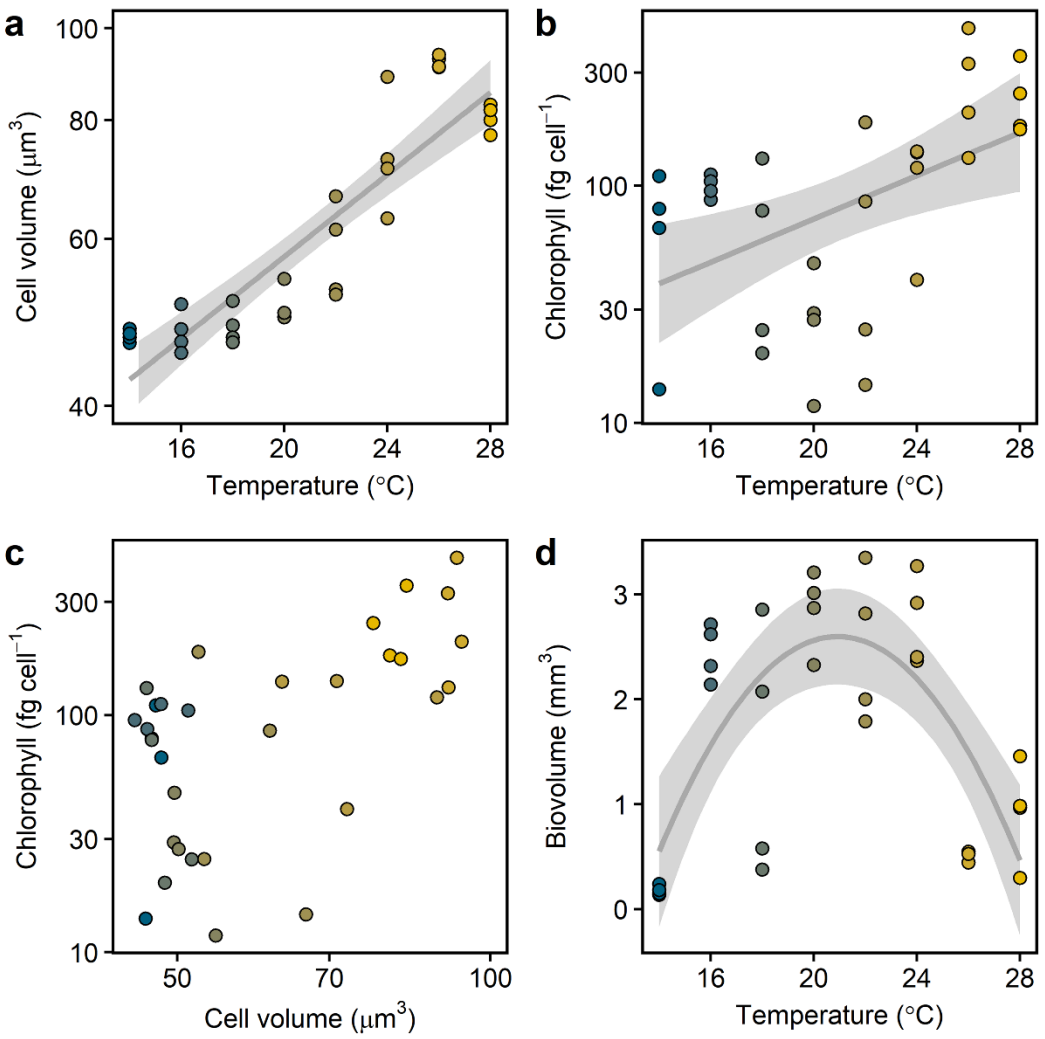
a
b
c
d
Cell volume (µm3)
Chlorophyll (fg cell−1)
Biovolume (mm3)
Temperature (°C)
Cell volume (µm3)
100
80
60
40
300
100
30
10
3
2
1
0
16
20
24
28
50
70
100

850

851

852

853

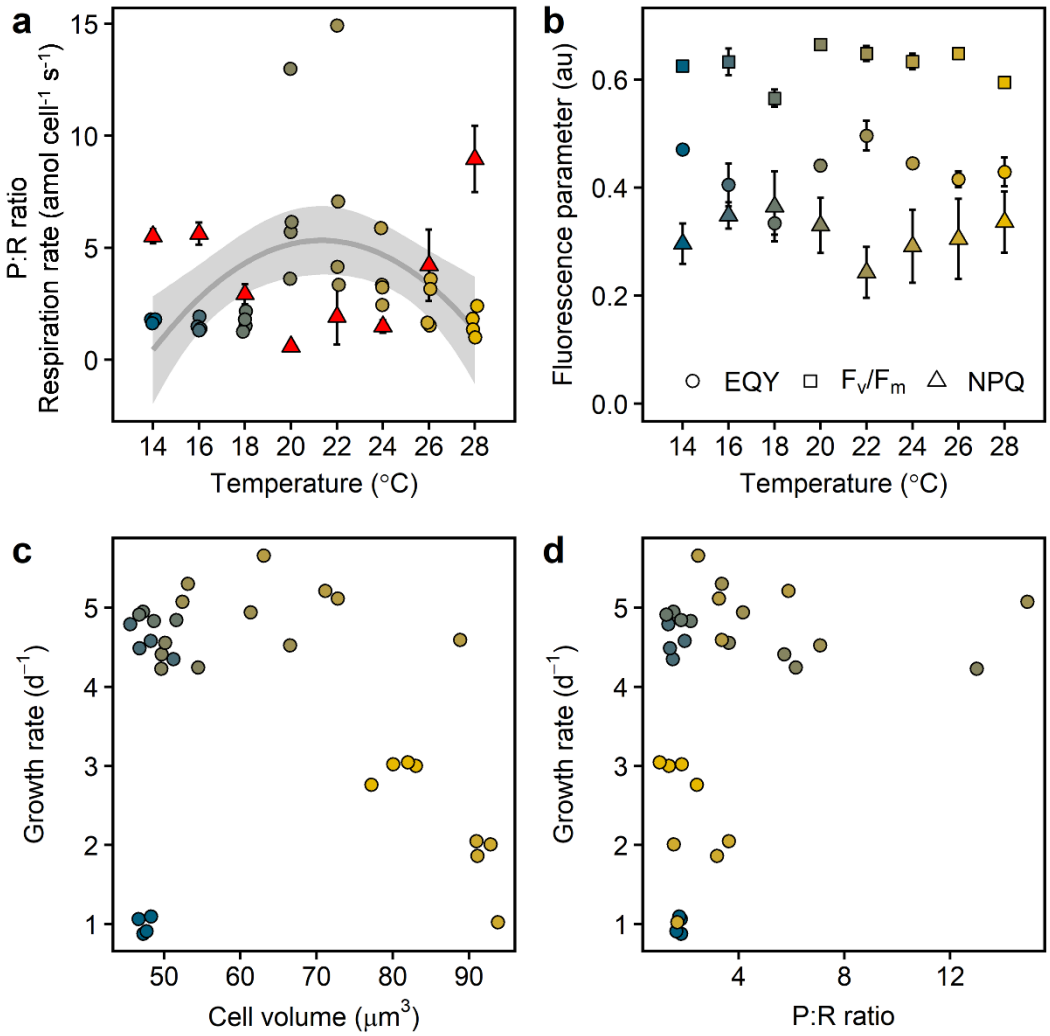
a
P:R ratio
Respiration rate (amol cell-1 s-1)
Temperature (°C)
b
Fluorescence parameter (au)
EQY
Fv/Fm
NPQ
Temperature (°C)
c
Growth rate (d-1)
Cell volume (µm3)
d
Growth rate (d-1)
P:R ratio

854

855

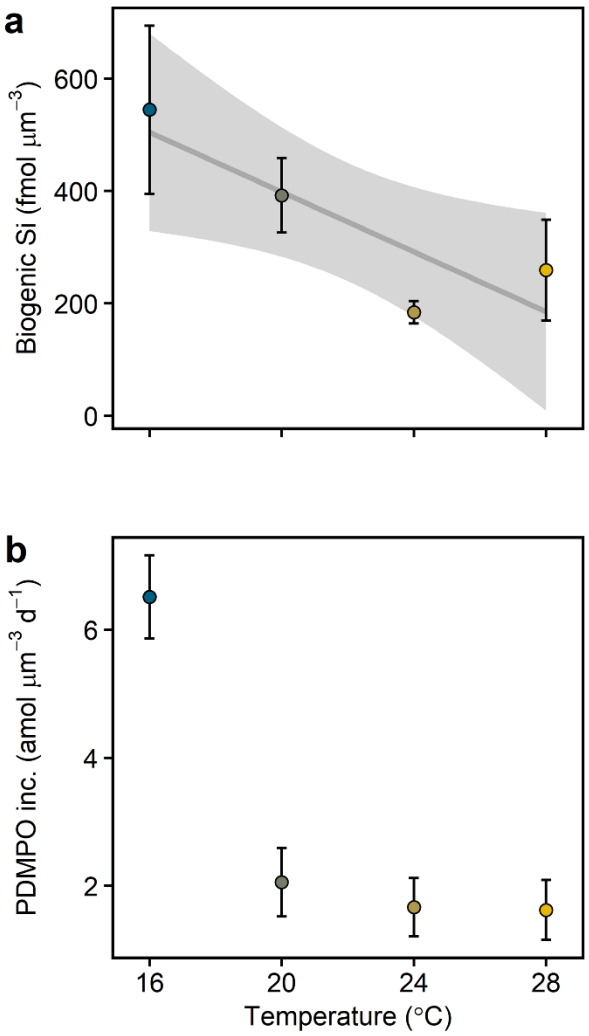
a
Biogenic Si (fmol µm^{-3})
600
400
200
0
b
PDMPO inc. (amol µm^{-3} d^{-1})
6
4
2
16
20
24
28
Temperature (°C)

856

857

858

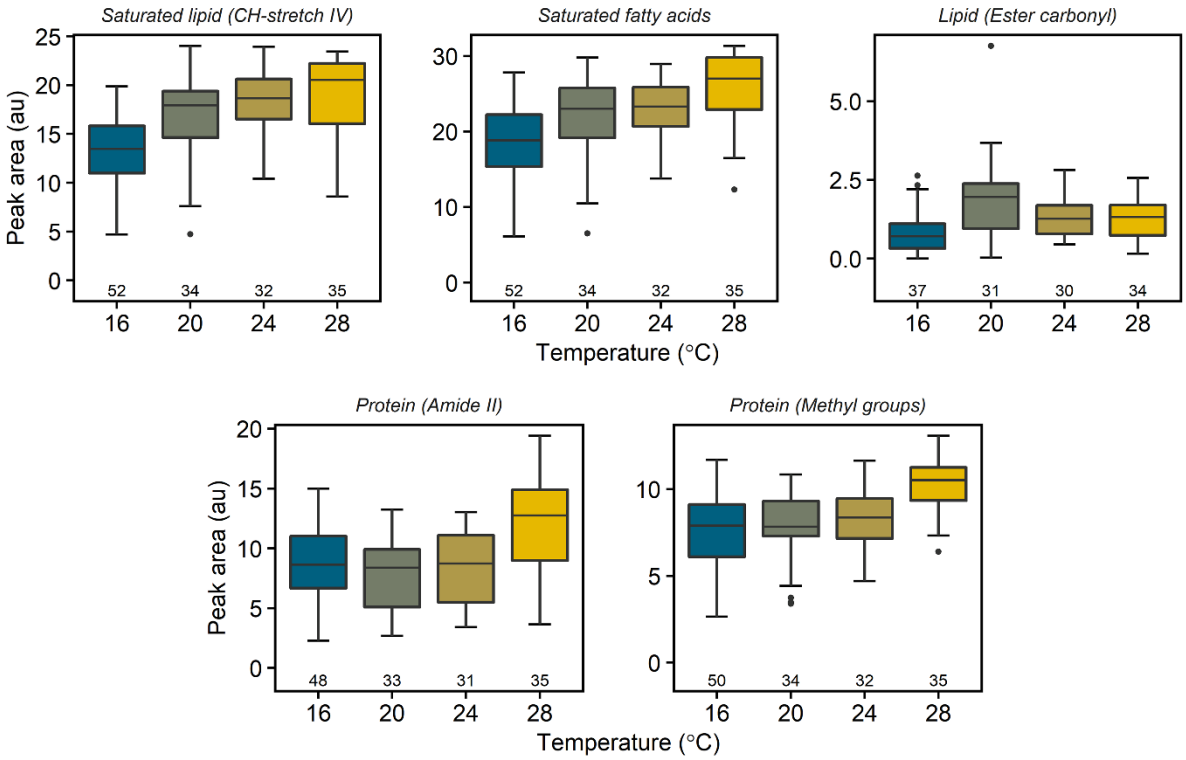
Saturated lipid (CH-stretch IV)
Saturated fatty acids
Lipid (Ester carbonyl)
Protein (Amide II)
Protein (Methyl groups)
Peak area (au)
Temperature (°C)
52 34 32 35
37 31 30 34
48 33 31 35
50 34 32 35
16 20 24 28

859

860

861

862

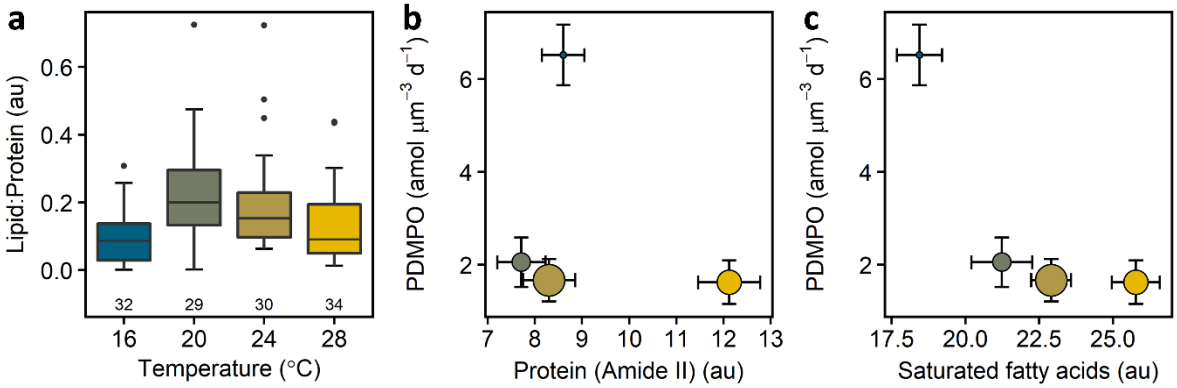
a
Lipid:Protein (au)
0.0
0.2
0.4
0.6
32
29
30
34
16
20
24
28
Temperature (°C)
b
PDMPO (amol µm−3 d−1)
2
4
6
7
8
9
10
11
12
13
Protein (Amide II) (au)
c
PDMPO (amol µm−3 d−1)
2
4
6
17.5
20.0
22.5
25.0
Saturated fatty acids (au)

863

864

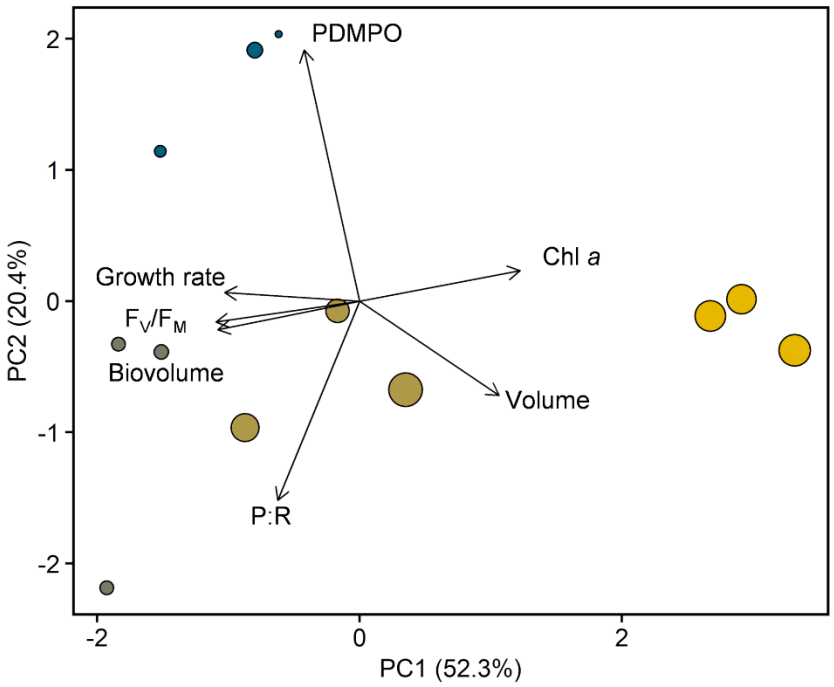
PDMPO
Chl a
Growth rate
F_V/F_M
Biovolume
Volume
P:R
PC2 (20.4%)
PC1 (52.3%)
2
1
0
-1
-2
-2
0
2

865